CHAPTER 3 : TWO COIL DESIGN

As shown in Chapter 2, the resistance of a single coil transducer increases while the inductance decreases as the dimensions of the coil are scaled down. This means that the coil has to be operated at higher frequencies for $\omega L \gg R$. Also, if used in the self-excited oscillator configuration, the high resistance causes the peak of the magnitude of impedance of the tank circuit versus frequency plot to decrease in amplitude and spread out making frequency measurement difficult. In order to get around this problem, a two coil planar transformer was investigated.

3.1.0 Measurements

Three two-coil transformer designs were investigated. The mask designs are shown in Fig. (3-1). All the coils had a line width of approximately 0.03 cm. The separation between adjacent lines (of two separate coils) was approximately 0.03 cm. The coils were fabricated on a copper PCB with a metal thickness of 17 μm. Large pads were chosen so as to minimize the effect of the contacts on the measurands. For the spiral coils, a copper wire was soldered from the center to the corresponding pad to complete the circuit.

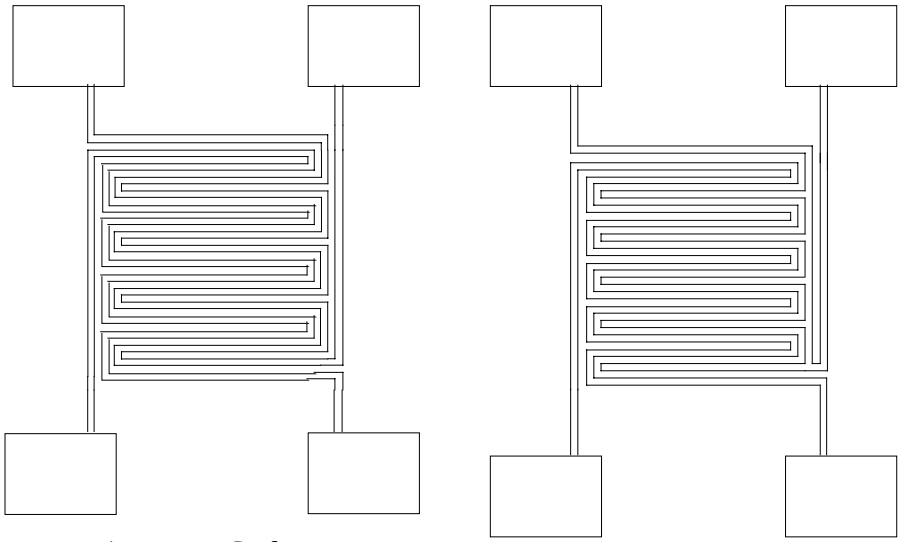

a) Zigzag Coil

b) Finger Coil

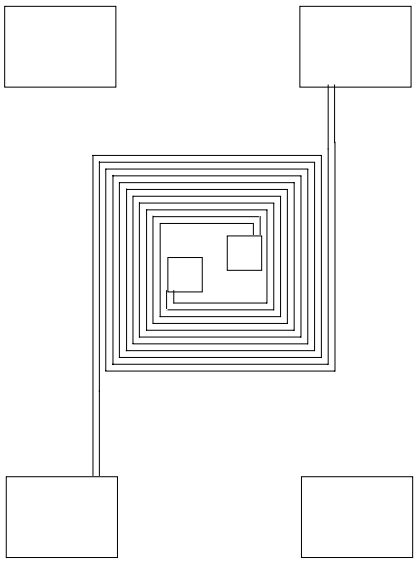

c) Spiral Coil

Fig. (3-1): Two-coil mask designs.

The test set-up to measure the gain and phase of the two-coil transformers is shown in Fig. (3-2). In the test set-up an oscillator output is applied to the primary of the two-coil planar transformer and the HP 4194A Gain/Phase Analyzer measures the gain and phase at the output (across the secondary coil) as the metal plate is brought closer to the transformer. Glass coverslips (thickness $\cong 0.015$ cm) and a glass slide (thickness $\cong 0.125$ cm) were inserted between the coils and a metal plate to simulate the effects of different gaps. The gain and phase at the output was measured for frequencies from 10 kHz to 40 MHz. As a compensation, the oscillator output was connected directly to the gain/phase analyzer.

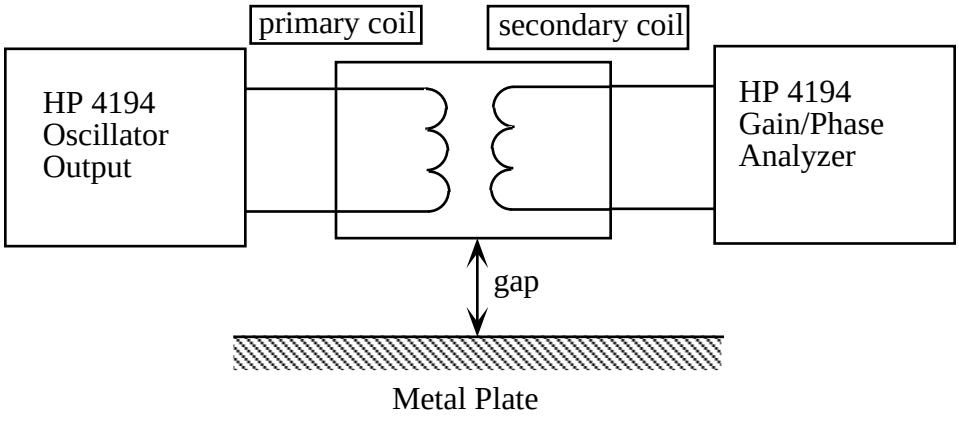

Fig. (3-2): Test set-up for measuring gain and phase of the voltage across the primary coil versus the output voltage across the secondary coil for different gaps between the coils and the plate.

Shown in Fig. (3-3), Fig. (3-4), Fig. (3-5) and Fig. (3-6) are the measured gain and phase plots. The solid lines (———) in all graphs correspond to the gain and phase of the two-coil planar transformer with no metal plate (or theoretically, the metal plate at infinity). The dotted lines (·····) correspond to the case where the distance

between the metal plate and the coils is approximately 0.125 cm. The dashed lines (— —) correspond to the case where the distance between the coils and the metal plate is approximately 0.015 cm.

Since the finger coils are not symmetrical, Fig. (3-4) corresponds to the case where the zigzag part of the finger coils is the primary coil and the digitate part of the finger coils is the secondary and Fig. (3-5) corresponds to the case where the digitate part of the finger coils is the primary and the zigzag part is the secondary. As can be seen from the plots, the two cases show a very similar response.

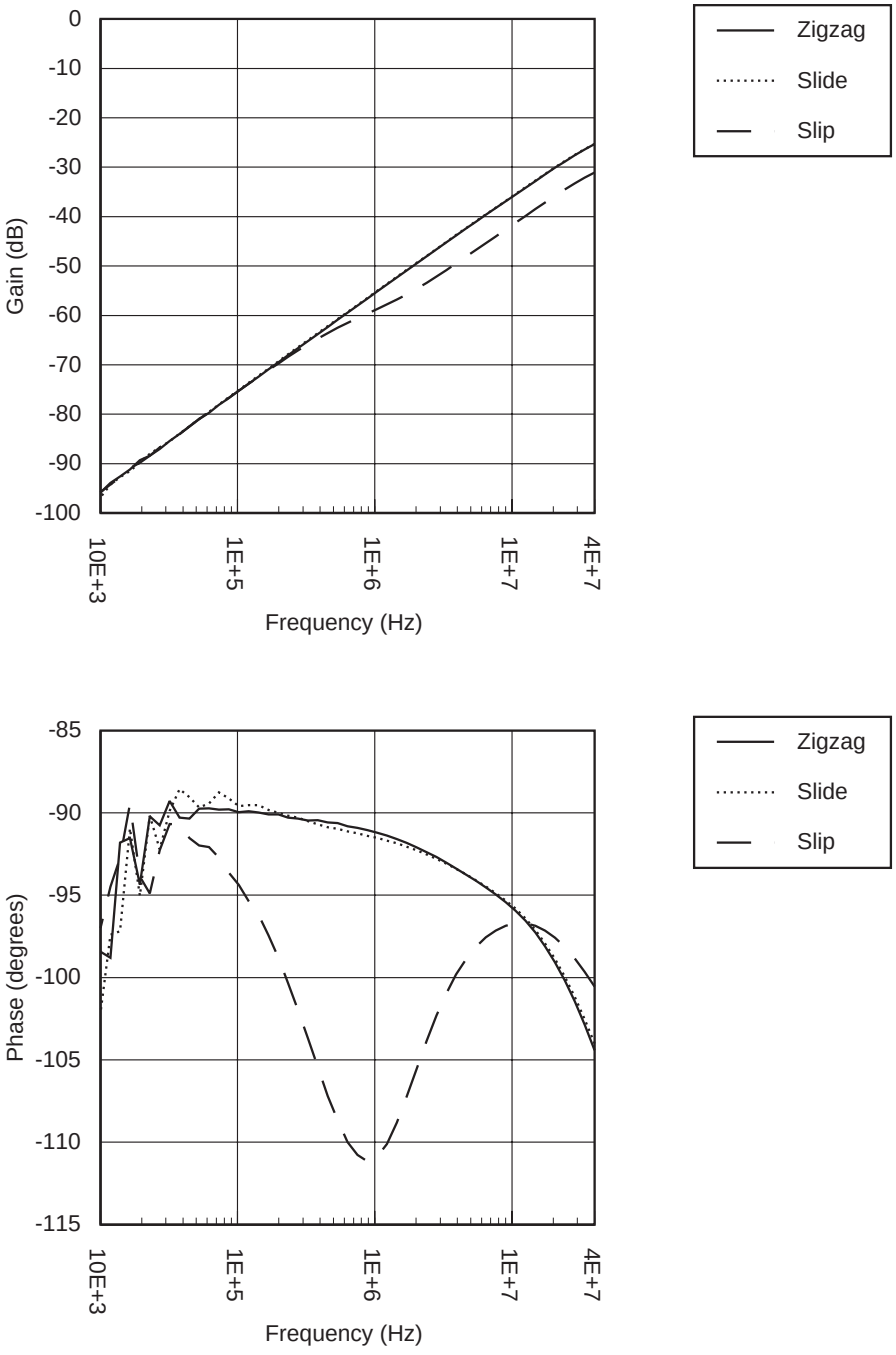

Fig. (3-3): Gain and phase measurements for the zigzag coil.

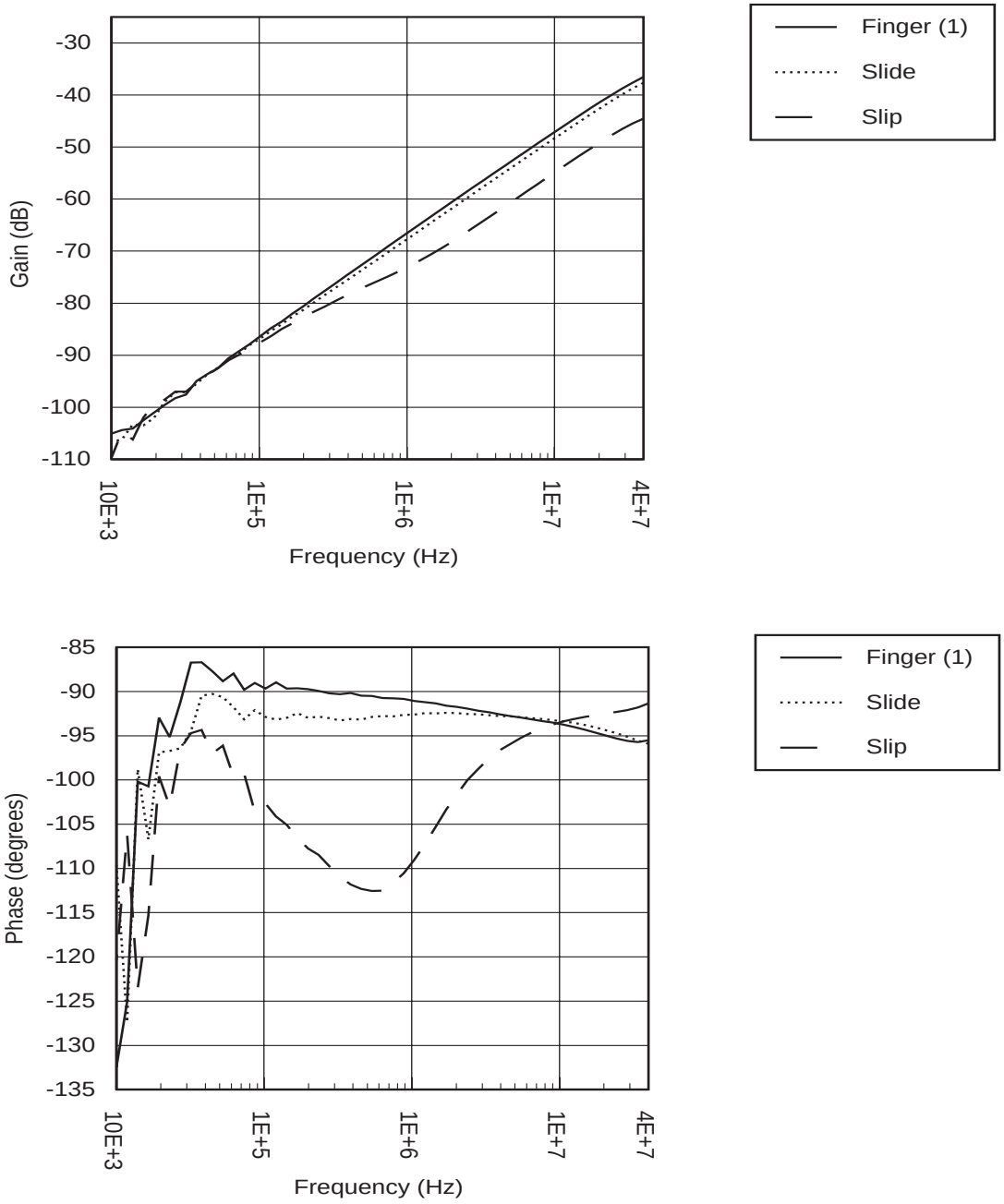

Fig. (3-4): Gain and phase measurement for the finger coil (1).

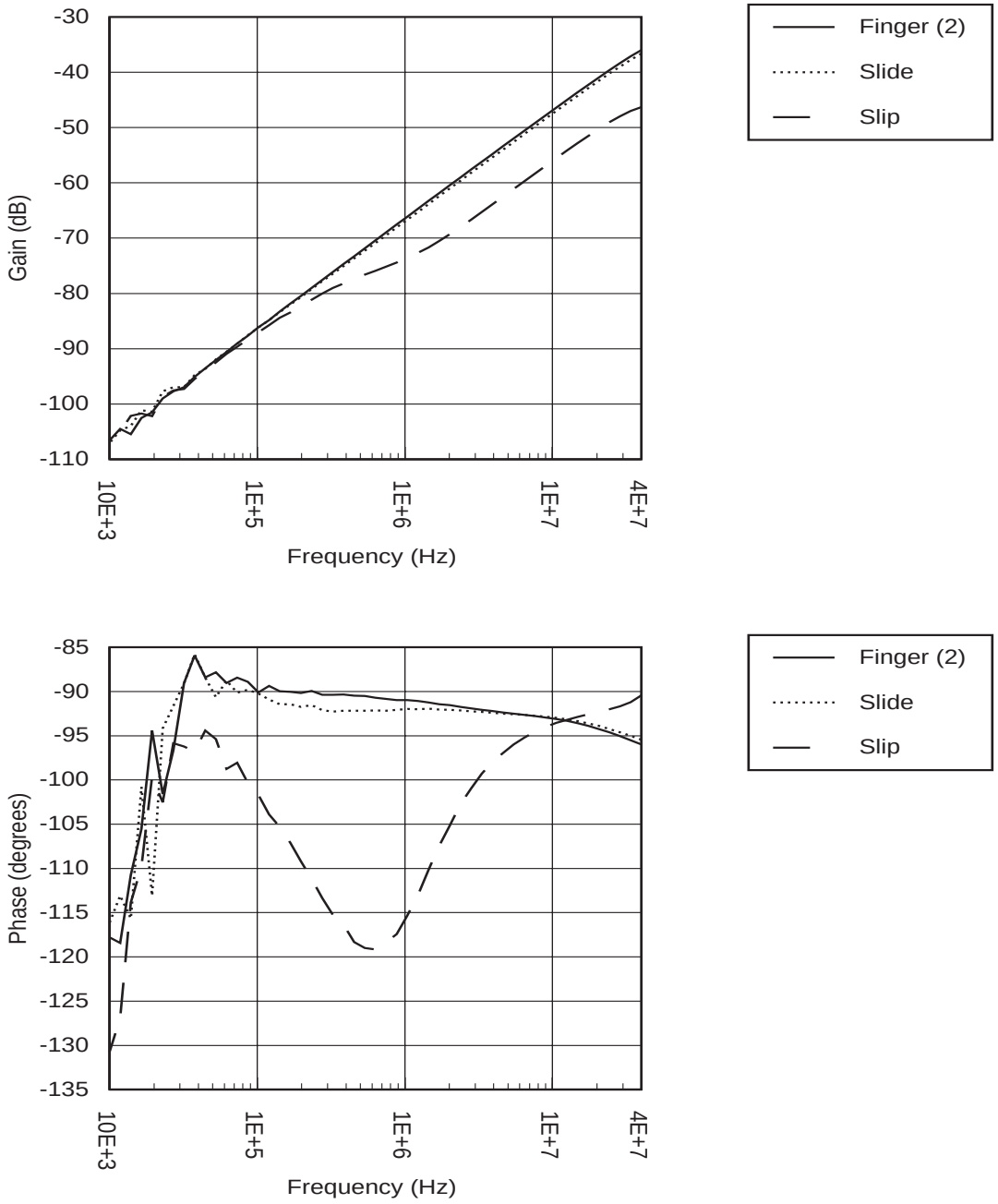

Fig. (3-5): Gain and phase measurement for finger coil (2).

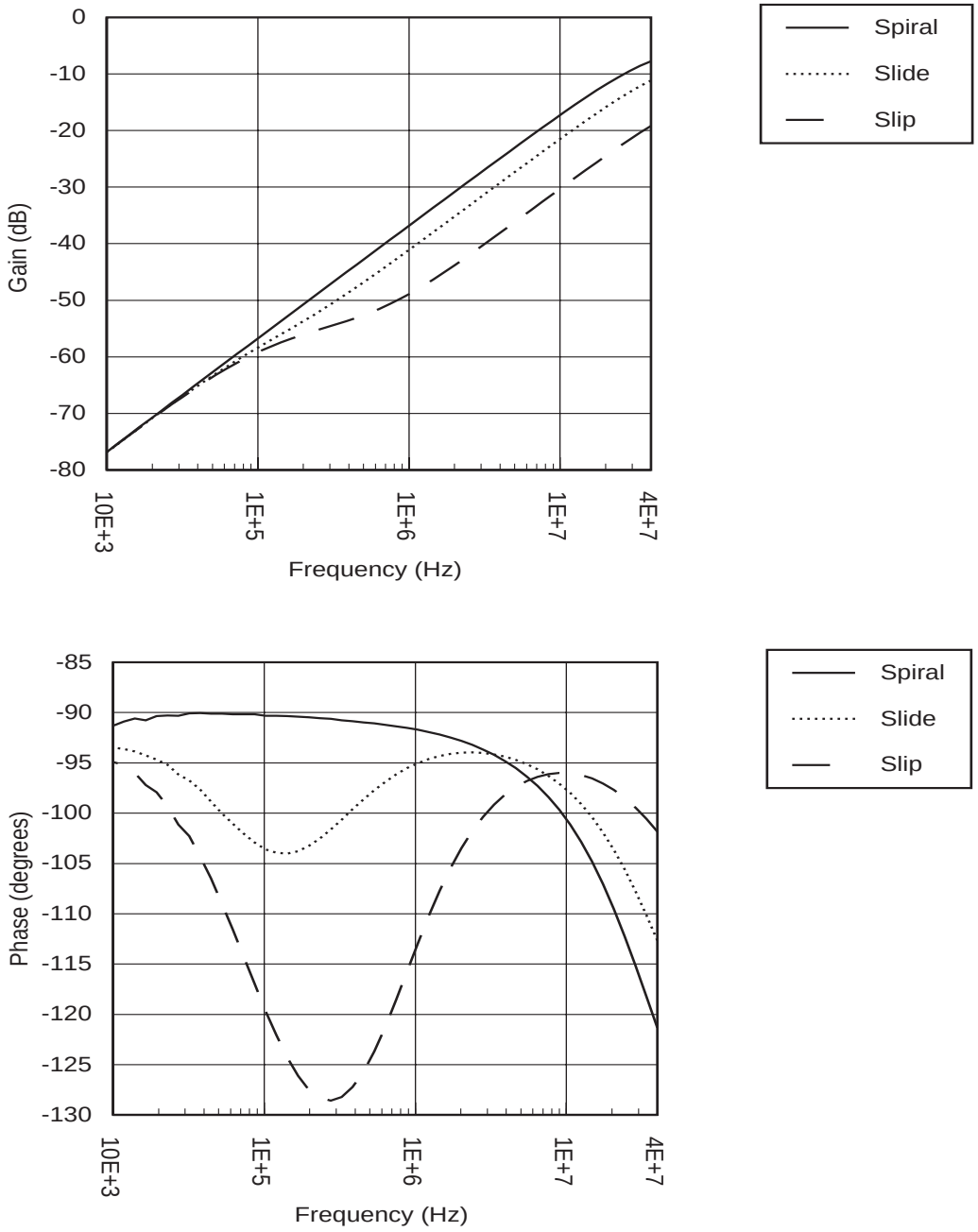

Fig. (3-6): Gain and phase measurement for spiral coil.

In all the cases the gain increases as the frequency increases. The gain for the spiral coil is the highest out of all the coils. It can also be seen from the graphs that there is a decrease in gain as the plate is brought closer to the coils.

In all the plots, the phase difference is approximately -90˚ for low frequencies with the plate at infinity. At higher frequencies, the phase difference increases in magnitude. This trend is more noticeable for the zigzag and the spiral coils. The more important feature of the phase plot is the dip produced in the plot as the plate is brought closer. This dip increases as the distance between the coils and the plate decreases. The dip occurs at approximately 100 kHz. This is approximately the same frequency at which the inductance of the single coil of same dimensions starts to change (spiral coil Fig. (2-7)). However measurements need to be performed at frequencies higher than 1 MHz for the greatest sensitivity in the case of a single coil. This means that the two-coil planar transformer type of transducer can be operated at lower frequencies to measure the same distances.

The spiral coil transducer was chosen as the best design since the change in phase as the distance between the plate and the coils changes, seems to be more linear than in the case of the fingers coils and the zigzag coils. The change in phase is also the largest for the spiral coils for a given distance between the plate and the coil. Also the gain for the spiral coils is the highest when compared to the other coils.

3.2.0 PSpice® Model

The spiral coil was chosen as the design to simulate since it gave the best results in the measurements. Shown in Fig. (3-7) is the PSpice® model used to simulate the situation of a planar transformer with the metal plate.

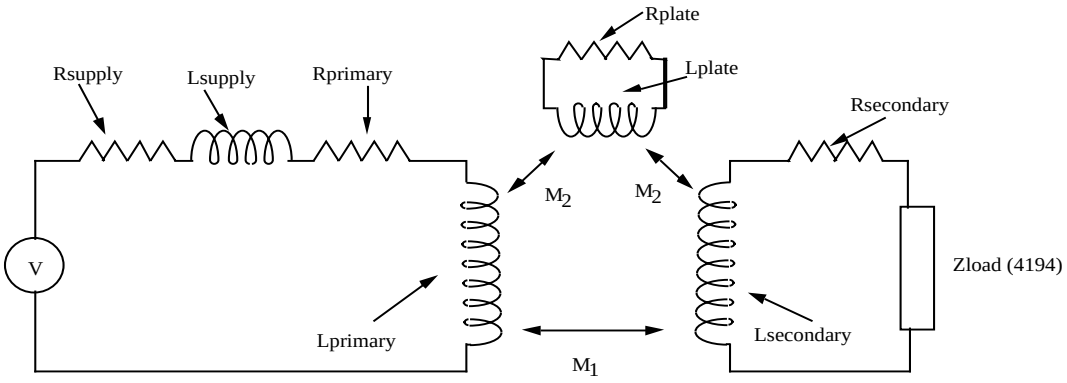

Fig. (3-7): PSpice® model for a two-coil planar transformer with the metal plate.

From Fig. (3-7), $L_{primary}$ and $R_{primary}$ are the inductance and resistance of the primary coil. $L_{secondary}$ and $R_{secondary}$ are the inductance and resistance of the secondary coil. Due to the symmetry of the spiral coils, $L_{primary} = L_{secondary}$ and $R_{primary} = R_{secondary}$. L_{plate} and R_{plate} are the effective inductance and resistance of the metal plate. The R_{plate} term includes the resistance of the plate and the discontinuity. L_{supply} and R_{supply} are the inductance and resistance of the driving circuit (which in this case was the HP4194A Gain/Phase Analyzer). Z_{load} is the load of the detection circuit (which in this case was the HP4194 Gain/Phase Analyzer again). M_1 is the mutual inductance between the two coils of the planar transformer. M_2 is the mutual inductance between the coils and the metal plate. Due to symmetry, the mutual inductance between the primary and the plate is equal to the mutual inductance between the secondary and the plate.

$L_{primary}$, $L_{secondary}$, $R_{primary}$, $R_{secondary}$, M_1 and M_2 can be calculated using the theo-

ries discussed in Chapter 2. Also, as shown previously, $L_{plate} = M_2$. Note that this means the inductance of the plate changes as the plate moves closer or further away from the coils. The only quantity which is yet to be determined is R_{plate}.

3.2.1 Calculation of R_{plate}

Shown in Fig. (3-8) is a model developed by Tuncer and Neikirk [1] to predict the behavior of a conductor over a ground plane. The paper shows that using this model, quasi-static analysis can predict the behavior of a transmission line with excellent agreement between the full-wave and static models over a wide range of frequencies and dimensions. By assuming a linearly spreading field with ‘h’, which is the gap between the conductor and the ground plane, the total impedance per unit length obtained using the quasi-static analysis was fitted to that obtained using the full-wave calculation. For a width of (w+6h) in the ground plane, the inductance calculated using the quasi-static model matched the full wave calculation very closely (within 3%) over a wide range of h/w (height-width ratio range).

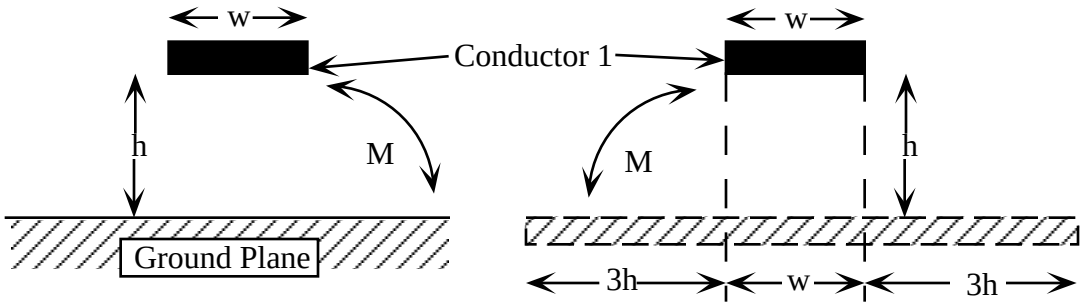

Fig. (3-8): The "w+6h" model developed by Tuncer and Neikirk, used to calculate R_{plate}.

This model replaces the conductor over the "ground plane" with a conductor over another conductor whose width is equal to (w+6h). The mutual inductance between the conductor '1' and the ground plane is equal to the mutual inductance between the conductor '1' and conductor '2'. Using this model, we can calculate R_{plate} using the width of (w+6h) as the width of the conductor as seen in the plate. As can be seen, the resistance of the plate changes as the plate is brought closer or further away from the conductor (coil). This phenomena also explains the change in inductance of the plate as the plate moves closer to or further away from the conductor (coil).

3.2.2 PSpice® Simulation

```
.PARAM ind = ?
.PARAM res =  ?

Vsupply 1 0 AC 1Volt

*******************************************************
*This is represents the effective internal impedance of the HP4194      *
*******************************************************
Rsupply 1 2a 50ohms
Lsupply 2a 2 65nH

***********************************
*This represents the transformer primary     *
***********************************
Rprimary 2 3 0.25ohms
Lprimary 3 0 88.46nH

*****************************************
*The following components are needed since PSpice *
*cannot evaluate the circuit with the floating plate      *
*****************************************
Ccoupling1 3 6 3pF
Rcoupling1 3 6 100Gohms

**********************
*This represents the Plate*
**********************
Lplate 8 6 {ind}
Rplate 6 8 {res}

Ccoupling2 8 4 3pF
Rcoupling2 8 4 100Gohms

***********************************
*This represents the transformer secondary*
***********************************
Lsecond 0 4 88.46nH
Rsecond 4 5 0.25ohms

*****************************************
*This is represents the effective load of the HP4194 *
*****************************************
Lload 5 5a 65nH
Rload 5a 0 50ohms
```

Fig. (3-9): PSpice® Simulation Program

```
*****
*M1*
*****
Kmutual1 Lprimary Lsecond 0.6715

*****
*M2.*
*****
Kmutual2 Lprimary Lplate {sqrt({ind}/88.46nH)}
Kmutual3 Lsecond Lplate {sqrt({ind}/88.46nH)}

.AC DEC 20 10KHz 40MegaHz
.Probe V(5)
.Print AC Vm(5) Vp(5)
.END
```

Fig. (3-9): PSpice® Simulation Program

The values given in the above program have been calculated using theories developed in Chapter 2. The only variables which can be used to match the experimental curves are the *coupling factor* (between the transformer and the plate) and R_{plate}. From PSpice®, the coupling factor [2] is equal to $\frac{M_2}{\sqrt{L_{primary}L_{plate}}}$. However since $M_2 = L_{plate}$, the equation is reduced to,

$$cf = \sqrt{\frac{L_{plate}}{L_{primary}}}, \qquad \text{Eq. (3-1)}$$

where 'cf' is the coupling factor. Note that for *Kmutual2* and *Kmutual3*, the coupling factors are equal since $L_{primary} = L_{secondary}$.

3.2.3 Effect of variations in $R_{primary}$ ($R_{secondary}$)

An important simulation using the PSpice® model is the variation in $R_{primary}$ (and $R_{secondary}$). Due to symmetry, they are equal. This simulation is particularly important

since as the coils are scaled down, the resistance of the coils increases dramatically while the inductance can be maintained at a few hundred nanohenries by increasing the number of turns in the coils and decreasing the spacing between segments. Shown in Fig. (3-10), are the results of the for the variation in $R_{primary}$ (and $R_{secondary}$) (▫ 0.01 Ω, ▪ 0.1 Ω, ⋄ 1 Ω, ◆ 10 Ω, x 100 Ω, ▶ 1000 Ω) with R_{plate} equal to 0.25 Ω and L_{plate} equal to 45 nH.

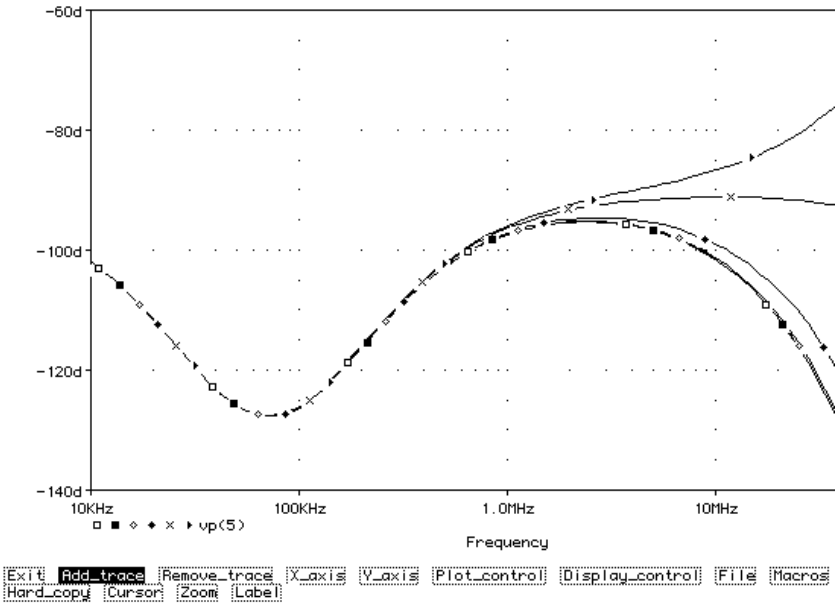

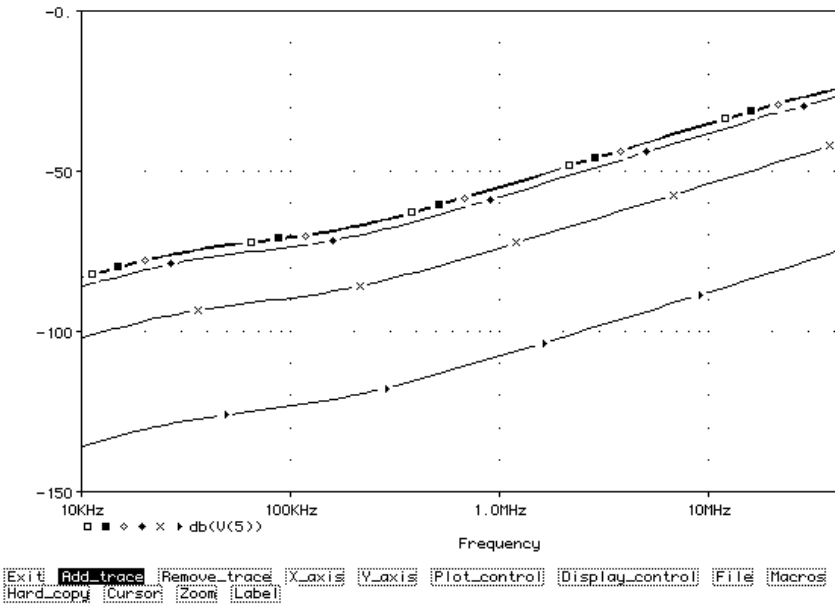

Fig. (3-10): Phase and gain plots for variation in Rprimary (and Rsecondary).

It can be seen that as the resistance increases the high frequency response of the circuit changes dramatically. More important however is the fact that the dip region of the phase plot remains unaffected for six orders of magnitude change in the resistance. However this is not without penalty. The gain decreases as the resistance increases.

3.2.4 Effect of variations in L_{plate} and R_{plate}

In the PSpice®model shown in Fig. (3-7), $L_{primary}$, $R_{primary}$, $L_{secondary}$ and $R_{secondary}$ can be calculated using models developed in Chapter 2. However, the coupling factor and R_{plate} can be used as fitting parameters in order to match the plots obtained using PSpice® to the experimental results. Since $M_2 = L_{plate}$, the coupling factor is a function of L_{plate} only, as shown in Eq. (3-1).

Shown in Fig. (3-11) is the PSpice® simulation for variation in L_{plate}. The value of R_{plate} is 0.05 Ω. L_{plate} varies from 20 nH to 50 nH in steps of 10 nH (▫ 20 nH, ▪ 30 nH, ◇ 40 nH, ◆ 50 nH).

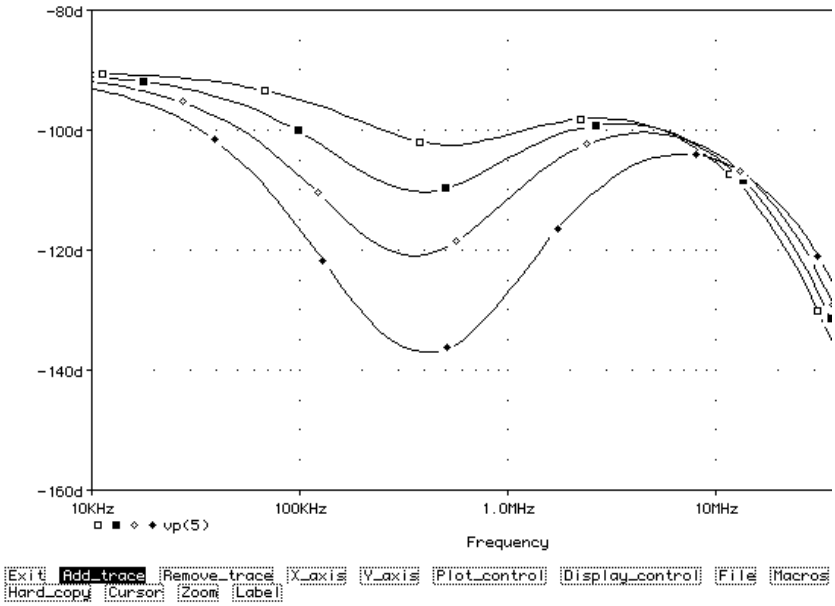

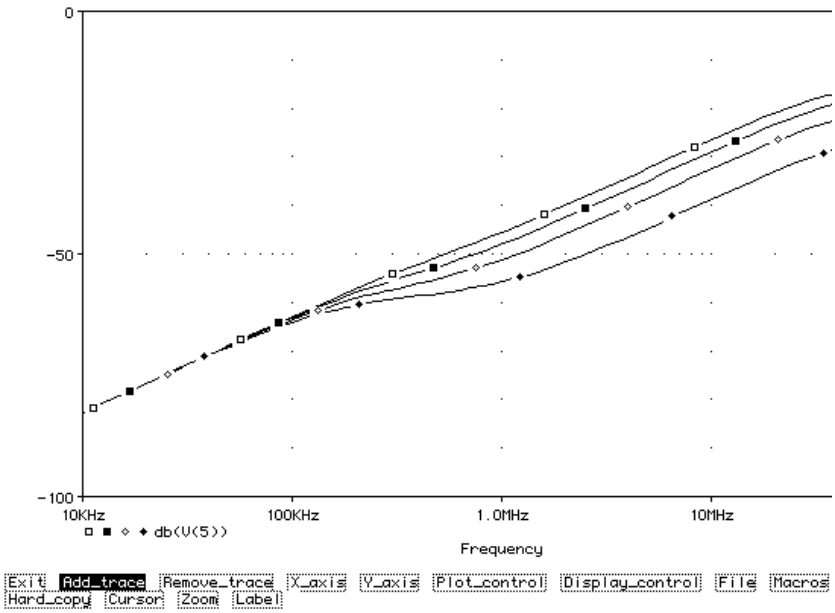

Fig. (3-11): Phase and gain plots (using PSpice®) for a variation in Lplate.

As can be seen from the plots, an increase in L_{plate} causes the dip in the phase plot to increase as the coupling factor is dependant on L_{plate}. In the gain plot, the effect of the change in L_{plate} is to cause a deviation at the frequency at which the dip in the phase plot occurs. This deviation increases as the value of L_{plate} increases.

Shown in Fig. (3-12) is the PSpice® simulation for variation in R_{plate}. The value of L_{plate} is equal to 45 nH. The R_{plate} is made to vary from 0.01 Ω to 0.04 Ω in steps of 0.01 Ω (▫ 0.01 Ω, ▪ 0.02 Ω, ◇ 0.03 Ω, ◆ 0.04 Ω).

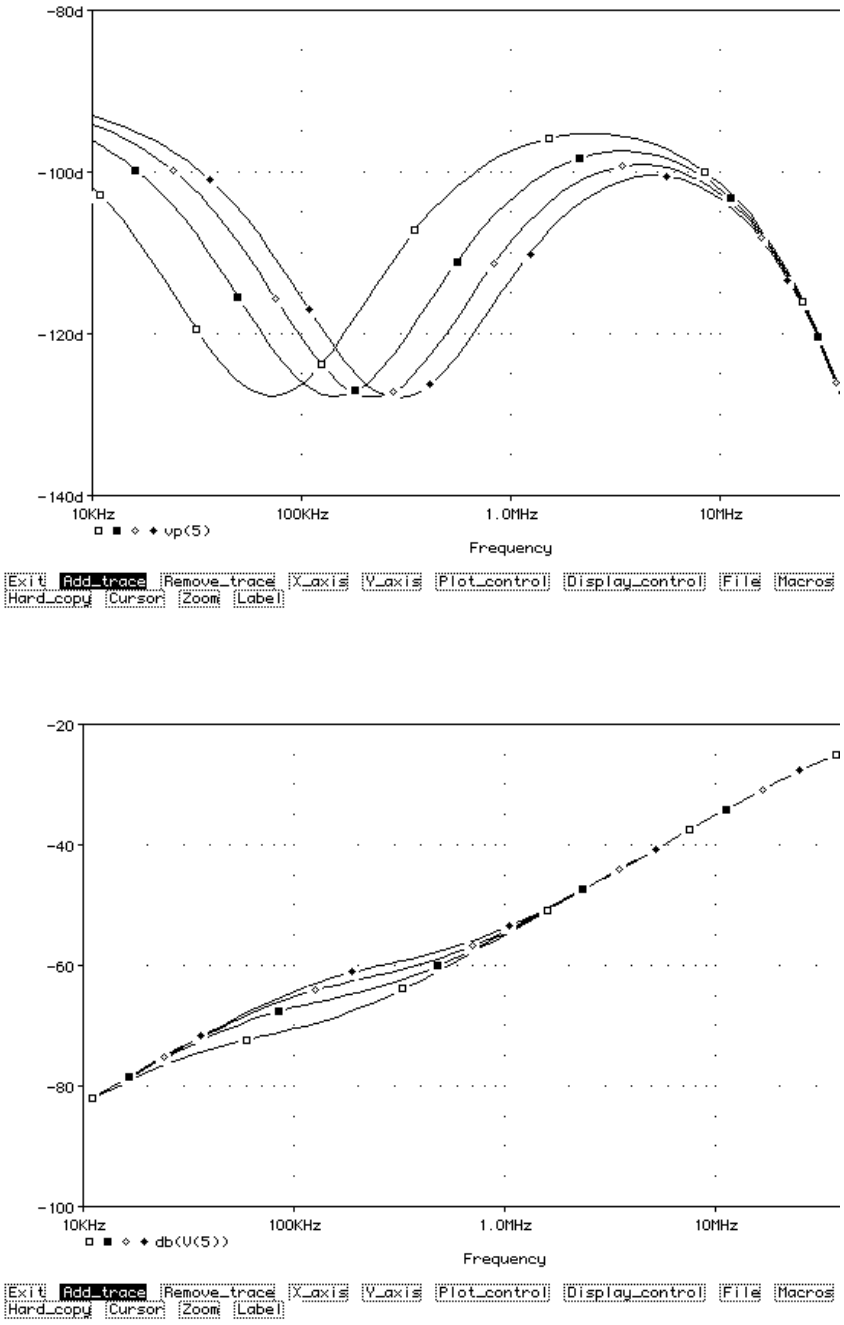

Fig. (3-12): Phase and gain plots (using PSpice®) for a variation in Rplate

As can be seen from the plots, a change in R_{plate} causes the dip in the phase plot to change in position. As R_{plate} increases, the dip in the phase plot moves towards higher frequencies. Note that the actual value of the phase at the dip for all the values of R_{plate} is the same. In the gain plot, a change in the R_{plate} causes the position of the deviation to change.

Thus from Fig. (3-11) and Fig. (3-12), we can adjust L_{plate} and R_{plate} to determine the values needed to fit the experimental curves (L_{plate} causes the dip to change in the y axis and R_{plate} causes the dip to move in the x axis).

3.2.5 Simulation results

The following values for $L_{primary}$, $R_{primary}$ and M_1 were computed using the theories developed in Chapter 2. $L_{primary}$ and $R_{primary}$ can also be experimentally determined by measuring the inductance and resistance of the primary coil using the HP 4194 Impedance/Gain-Phase Analyzer with the secondary open as shown in Fig. (3-13).

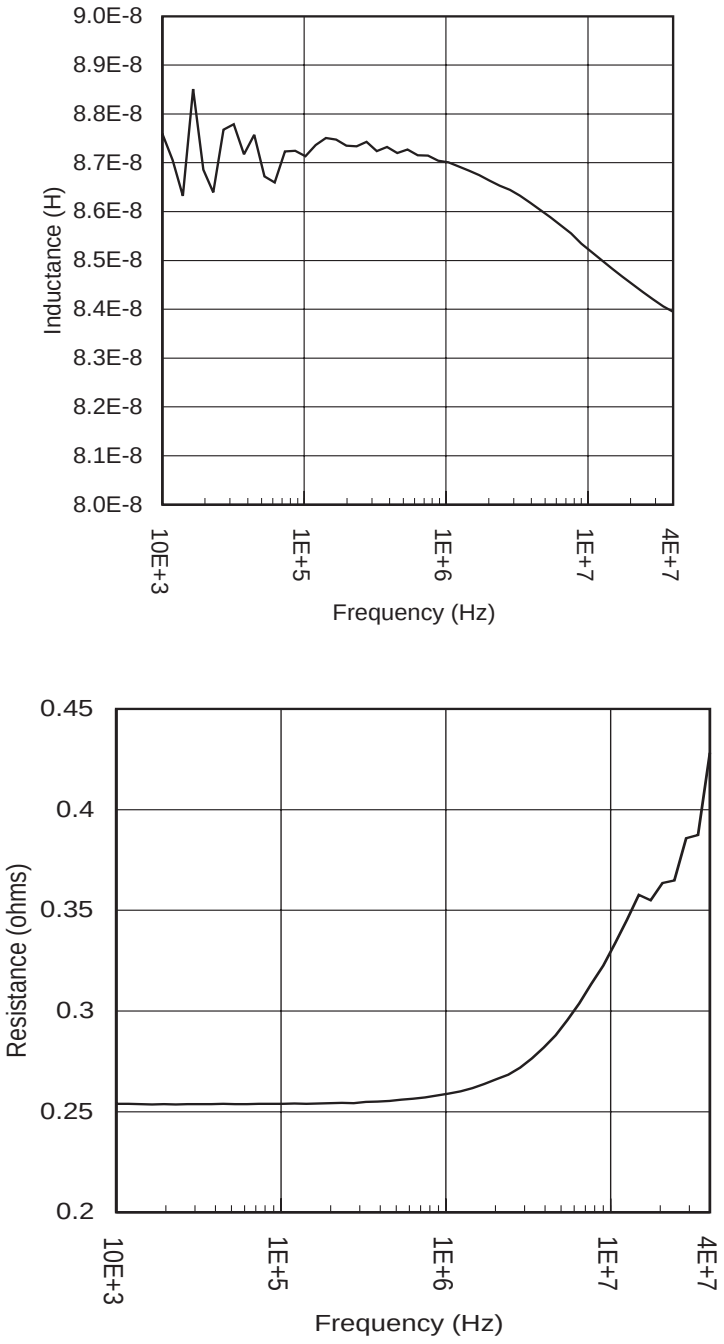

Fig. (3-13): Inductance and resistance graphs for the primary coil with the secondary coil open.

$R_{primary} = R_{secondary} = 0.25\ \Omega$

$L_{primary} = L_{secondary} = 88$ nH

$M_1 = 59$ nH ($coupling\ factor = \frac{M}{\sqrt{L_1 L_2}} = \frac{59}{\sqrt{88\,(88)}} = 0.67$)

Using the above computed values in the PSpice® model, the following values of L_{plate} and R_{plate} were obtained by matching the PSpice® plots with the experimental graphs.

Gap (cm)	L_{plate} (nH)	R_{plate} (Ω)
0.015	44.9	0.0337
0.030	39.5	0.0288
0.060	31.3	0.0226
0.090	25.4	0.0177
0.120	21.0	0.0146

Fig. (3-14): PSPice® values to match the experimental graphs

L_{plate} was also determined by calculating M_2 (the mutual inductance between the plate and the coil) since $L_{plate} = M_2$. R_{plate} was also calculated using the theories developed by Tuncer and Neikirk.

Shown in Fig. (3-15) is the comparison between the values for L_{plate} and R_{plate} obtained using the PSpice® model and those obtained using calculations.

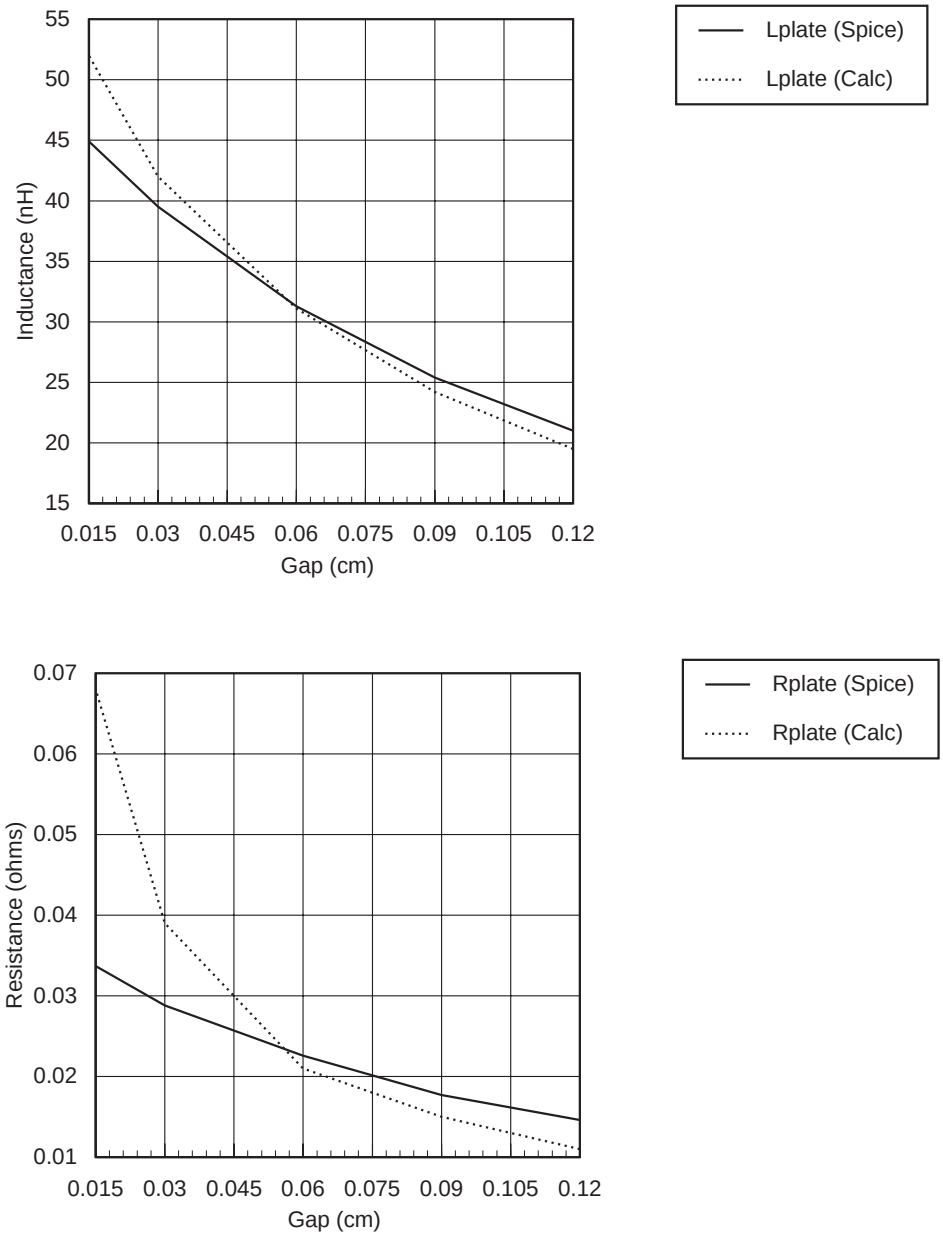

Fig. (3-15): PSpice® vs. calculated values for L_{plate} and R_{plate}

It can be seen that the calculated inductance matches values obtained from the

PSpice® model very well. The calculated resistance however deviates from the PSpice® model resistance, for small gaps.

Thus as the coils are scaled, we can calculate the various component values needed for the circuit model using theories developed in Chapter 2 (for $L_{primary}$, $L_{secondary}$, $R_{primary}$, $R_{secondary}$ and L_{plate}) and Chapter 3 (for R_{plate}). These component values can then be plugged into a PSpice® program to simulate the performance of an actual two-coil transformer type transducer for the eddy current sensor.

3.3.0 Circuit

With the model of the transducer for an eddy-current sensor complete, we need to focus on the sense and driving circuit needed for the two-coil transducer. Since the phase between the input voltage across the primary coil and the output voltage across the secondary coil changes with gap between coils and plate, we need to design a phase detection circuit. Shown in Fig. (3-16) is the block diagram of the phase detection circuit [3]. The primary of the planar transformer is excited using an oscillator. This oscillator also provides a reference signal to the phase detector circuit. The output across the secondary coil is amplified and provided as the other input to the phase detection circuit. The phase detection circuit measures the phase difference between the reference signal and the output signal.

As can be seen from phase measurements for the spiral coil (Fig. (3-6)) the operating range of the frequency is very narrow. Thus ideally an oscillator that produces a relatively clean sine wave is needed [4]. Since sine wave oscillators are difficult to build monolithically, the oscillator can be built off-chip and the signal to the primary could be provided through lead wires. The phase shift provided by the lead wires would be nulled since the same signal is provided to the primary and the phase detector. The

phase detector, however, would be needed to be built close to the secondary output (monolithically with the transducer) so as to eliminate any phase shift that would be produced if lead wires were attached to the secondary.

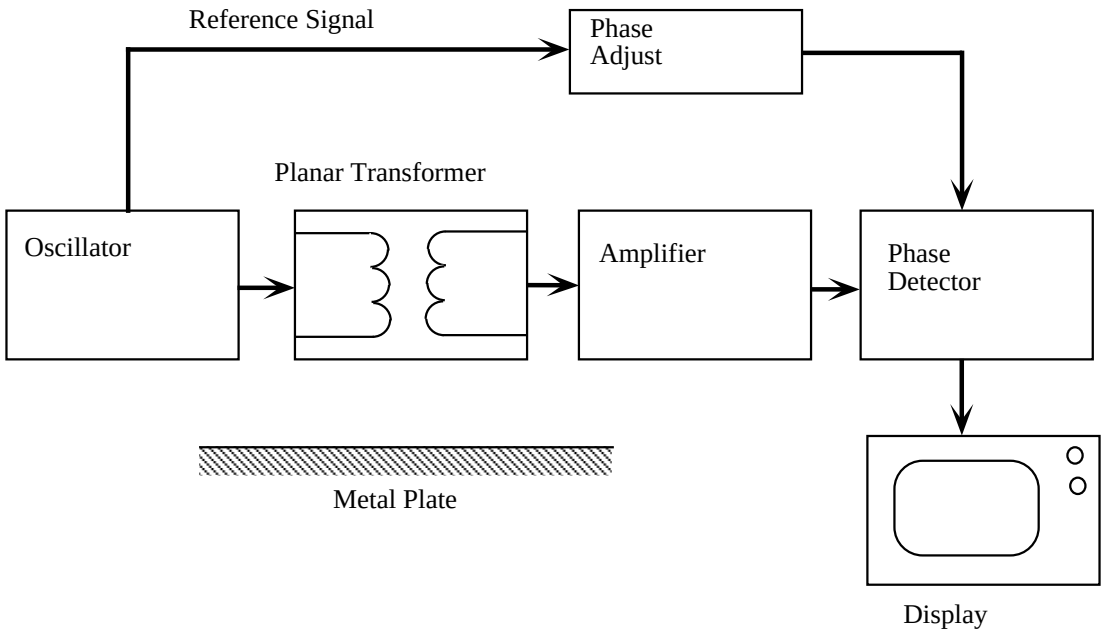

Fig. (3-16): Block diagram for phase detection circuit

3.4.0 Potential Applications

3.4.1 An Electromagnetic Accelerometer

An electromagnetic accelerometer using a single coil has already been demonstrated [6]. The same accelerometer can be fabricated using the two-coil design. Fig. (3-17) shows a schematic diagram of the accelerometer. The plate is placed on a seismic mass (or proof mass) which is fabricated at the end of a cantilever beam. The coils are placed under the plate on the substrate below. The seismic mass causes the cantilever to bend under the force produced due to acceleration. This moves the plate closer or further away from the coils. Again, the change in phase between the input across the primary and the output across the secondary with change in gap can be used as a measure of the acceleration.

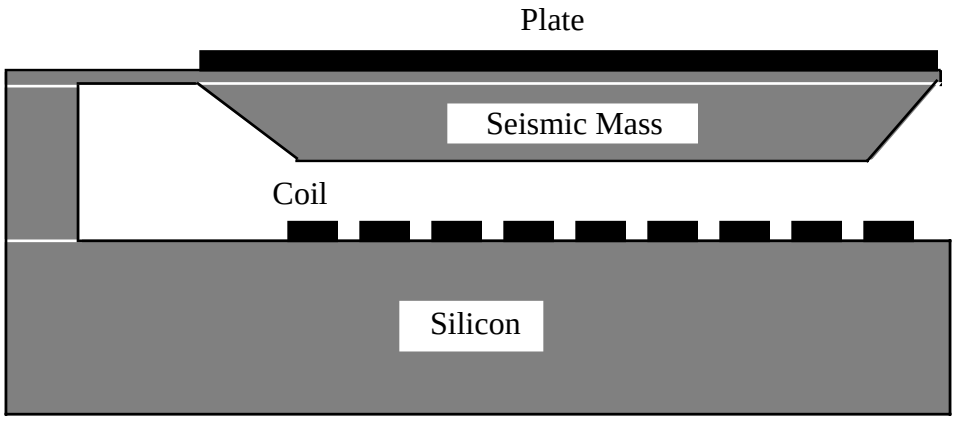

Fig. (3-17): An accelerometer

3.4.2 An Electromagnetic Bearing Wear Sensor

An ultrasonic bearing wear sensor has been demonstrated by J. C. Chan [5]. A version

which uses the two-coil design is shown in Fig. (3-18). The metal plate, in this case, is placed at fixed distance from the planar coils. As the bearing rotates, the friction between the outer sleeve and the bearing causes bearing wear. Since the metal plate is incorporated into the outer sleeve, it too wears out (becomes thinner) due to the friction between the rotating bearing and itself. This causes the resistance of the plate to increase. The effect of change in plate resistance on the phase is shown in Fig. (3-12). Thus by measuring the phase difference at a given frequency the resistance of the plate can be measured which in turn gives a measure of the wear produced in the bearing.

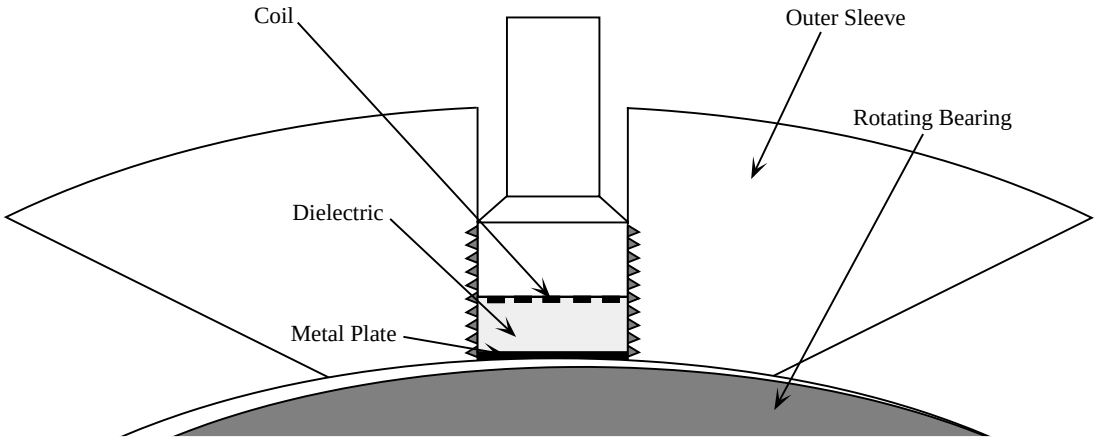

Fig. (3-18): Bearing wear sensor

3.5.0 Summary

This chapter discusses the different two-coil designs. The gain and phase measurements for the different designs are shown. The spiral coils were judged as the best design. The PSpice® model for the two-coil planar transformer with the plate is shown. Calculations for the various component values are discussed. Using the

PSpice® model the effect of variations in component values is explored. It is seen that the transducer output (phase) is relatively insensitive to variations in the resistance of the coils. The phase detection circuit is also discussed. Finally potential applications for the two-coil planar transformer are shown.

References

[1] E. Tuncer, and D. P. Neikirk, *Highly Accurate Quasi-static Modeling of Microstrip Line Over Lossy Substrates*, IEEE Microwave and Guided Wave Letters, vol. 2, pp. 409, 1992.

[2] P. W. Tuinenga, *Spice: A guide to Circuit Simulation and Analysis using PSpice*, New Jersey: Prentice Hall, 1992.

[3] H. L. Libby, *Introduction to Electromagnetic Nondestructive Test Methods*, Wiley-Interscience, 1971.

[4] Discussions with D. Neikirk, 1994

[5] J. C. Chan, *On-Line Ultrasonic Monitoring of Bearing Wear*, Turbomachinery International, pp. 12, Nov/Dec, 1990.

[6] E. Abbaspour-Sani, R.-S. Huang, and C. Y. Kwok, *A Novel Electromagnetic Accelerometer*, Electron Device Letters, vol. 15, pp. 272, 8 1994.